Nanoscale

ROYAL SOCIETY OF CHEMISTRY

PAPER

View Article Online
View Journal | View Issue

Cite this: *Nanoscale*, 2025, **17**, 18744

Zinc complex-based multifunctional binders for lithium sulfide-based lithium–sulfur batteries†

Zhe Huang, Yonglin Wang, Yixuan Zhao and Yuning Li *

Lithium sulfide (Li_2S) is a promising cathode material for lithium–sulfur batteries (LSBs) due to its compatibility with lithium-free anodes and commercial electrode processing. However, its high moisture sensitivity and processing difficulties pose challenges, particularly in identifying suitable binders. Here, we report a fluorine-free binder based on a zinc acetate triethanolamine ($Zn(OAc)_2$·TEA) complex, which exhibits enhanced specific capacity, rate capability, and cycling stability compared to the commonly used PVDF binder. These improvements are attributed to the strong lithium polysulfide (LPS) trapping ability and redox catalytic activity of the $Zn(OAc)_2$·TEA complex. To improve mechanical robustness and solution stability, polyethylenimine (PEI) was incorporated to form a $Zn(OAc)_2$·TEA/PEI hybrid binder. Electrochemical testing revealed that Li_2S cathodes employing $Zn(OAc)_2$·TEA/PEI with 10 wt% PEI delivered superior rate performance, high discharge capacity, and excellent long-term cycling stability. This work presents a promising fluorine-free binder strategy that integrates LPS trapping and redox catalysis, advancing the practical development of high-performance Li_2S-based LSBs.

Received 13th May 2025,
Accepted 20th July 2025

DOI: 10.1039/d5nr01950h

rsc.li/nanoscale

1. Introduction

The increasing demand for high-energy-density rechargeable batteries has driven significant efforts to improve conventional lithium-ion batteries (LIBs) and to develop next-generation battery technologies.[1–9] Among emerging candidates, lithium–sulfur batteries (LSBs) have attracted considerable attention due to sulfur's natural abundance and their exceptional theoretical specific energy of 2600 W h kg^{-1}, which is approximately five times that of LIBs.[10,11]

Conventional LSBs that use elemental sulfur as the cathode active material, referred to as S-LSBs, rely on metallic lithium or lithium alloy anodes,[12] which are highly reactive with oxygen, nitrogen, and moisture, posing serious safety concerns during manufacturing and raising the production cost of these batteries. Moreover, lithium metal anodes are prone to dendrite formation, which can lead to short circuits, thermal runaway, and even explosions.[13–15] To overcome these limitations, Li_2S has been explored as an alternative cathode material. Its use enables pairing with safer Li-free anode hosts like graphite,[16] silicon,[17] and tin,[18] while offering greater compatibility with existing LIB manufacturing processes, making Li_2S-based LSBs (Li_2S-LSBs) more viable for commercial application.[19–21]

Despite these advantages, Li_2S-LSBs introduce new challenges. Notably, Li_2S is highly sensitive to moisture and has a high melting point, which complicates electrode fabrication compared to elemental sulfur-based cathodes.[22–24] One critical component affected by these constraints is the binder. Due to the hydrolytic reactivity and basicity of Li_2S, water- or acid-based binders commonly used in S-LSBs are unsuitable. Consequently, the number of binders reported for Li_2S-LSBs remains limited (Table S1†) in contrast to the wide array available for S-LSBs.[25–27] Poly(vinylidene fluoride) (PVDF), the most widely used binder for S-LSBs,[28] is also the most commonly adopted for Li_2S-LSBs due to its excellent electrochemical stability. However, our recent findings revealed that PVDF undergoes dehydrofluorination when mixed with Li_2S during slurry processing. This reaction consumes Li_2S and degrades PVDF's binding performance, leading to poor electrochemical performance.[23] Furthermore, growing environmental concerns have prompted regulatory bodies, such as the European Union, to propose restrictions or bans on fluorinated polymers including PVDF and PTFE,[29,30] emphasizing the urgent need for fluorine-free binder alternatives for Li_2S-LSBs.

Li_2S-LSBs also face several challenges similar to S-LSBs, including the formation of soluble lithium polysulfides (LPSs) that induce a shuttle effect and result in rapid capacity fading, as well as the inherently poor electronic and ionic conductivities of solid sulfur species, which lead to sluggish reaction kinetics.[15,22] Although various strategies, such as

Department of Chemical Engineering and Waterloo Institute for Nanotechnology (WIN), University of Waterloo, 200 University Ave West, Waterloo, Ontario N2L 3G1, Canada. E-mail: yuning.li@uwaterloo.ca

† Electronic supplementary information (ESI) available. See DOI: https://doi.org/10.1039/d5nr01950h

incorporating functional additives into the cathode, have been developed to address these issues in S-LSBs, many are not directly applicable to Li_2S-LSBs due to the above-mentioned high chemical reactivity of Li_2S.[31–37]

In recent years, the design and development of functional binders have been recognized as a critical strategy to address the challenges of both S-LSBs and Li_2S-LSBs. Beyond providing mechanical integrity, advanced binders play an active role in enhancing cathode performance by improving electronic conductivity, immobilizing LPSs, and catalyzing redox reactions. Various innovative approaches, such as chemical functionalization, incorporation of polar or redox-active groups, and the development of hybrid binder systems, have been explored to achieve these goals.[38–40] Despite these advances, current binder systems still face significant limitations such as insufficient mechanical resilience at high sulfur loadings, limited long-term chemical stability, and trade-offs between adhesion strength and flexibility. These progresses and remaining challenges have been thoroughly reviewed in a recent article,[41] which highlight the importance of multifunctional binder design for improving the electrochemical stability and cycling life of S-LSBs and Li_2S-LSBs.

Previously, our group demonstrated that zinc acetate diethanolamine ($Zn(OAc)_2$·DEA) complex can serve as a low-cost, fluorine-free binder in both lithium iron phosphate (LFP) batteries and S-LSBs.[42,43] Its strong binding capability arises from the flexible DEA ligand and multiple hydrogen bonding sites. Importantly, this complex can also function as a LPS trapper to suppress shuttle effect and a catalyst to promote redox reactions in S-LSBs, enhancing cycling stability and rate capability.[42]

Motivated by these results, we explored the feasibility of applying $Zn(OAc)_2$·DEA complex as a binder in Li_2S-LSBs. However, the hydrolytic nature of Li_2S necessitates strictly anhydrous processing with dry reagents and solvents. Initially, we synthesized a $Zn(OAc)_2$·DEA solution in anhydrous ethanol and used it to prepare Li_2S slurries. This approach proved unsuitable, as partially dissolved Li_2S in ethanol rapidly reacted with the $Zn(OAc)_2$·DEA complex, leading to immediate gelation. To resolve this, we attempted to use anhydrous *N*-methyl-2-pyrrolidone (NMP), a widely used battery processing solvent and is known for its stability with Li_2S.[23] However, $Zn(OAc)_2$·DEA exhibited poor solubility in NMP. To address this, we substituted DEA with triethanolamine (TEA), introducing an additional $-CH_2CH_2OH$ group. This modification enabled successful synthesis of $Zn(OAc)_2$·TEA directly in anhydrous NMP, and the resulting solution can be used directly as a binder solution to prepare the Li_2S cathode composite. The $Zn(OAc)_2$·TEA-based cathode demonstrated markedly improved cycling stability at 0.1 C upon initial activation and high rate performance compared to the PVDF-based electrode.

To further improve the solution stability of $Zn(OAc)_2$·TEA and mechanical robustness of the Li_2S-based electrodes, a small amount (10 wt%) of polyethylenimine (PEI) was added into the $Zn(OAc)_2$·TEA solution. The resulting $Zn(OAc)_2$·TEA/PEI (10%) complex serves as an efficient, fluorine-free binder for Li_2S-LSBs, enabling improved electrode integrity, excellent cycling stability, and high-rate performance.

2. Materials and methods

2.1 Materials

Lithium sulfide (Li_2S, 99.98% trace metals basis), zinc acetate dihydrate ($Zn(OAc)_2·2H_2O$, ACS reagent, ≥98%), diethanolamine (DEA, ACS reagent, ≥98.5%), triethanolamine (TEA, ≥99.5%), polyethylenimine (PEI, M_w ~25 000 by LS, M_n ~10 000 by GPC, branched), anhydrous ethanol (EtOH, ≤0.003% water), and anhydrous *N*-methyl-2-pyrrolidone (NMP, 99.5%) were purchased from Sigma-Aldrich. Super P (SP) was purchased from IMERYS. Polyvinylidene fluoride (PVDF, M_w ~1 000 000) was from Kynar. The commercial anhydrous EtOH was further dried using 3 Å molecular sieves. Anhydrous NMP was further dried using lithium metal and filtered through a PTFE syringe filter before use. All other chemicals were used as received without further purification.

2.2 Synthesis of $Zn(OAc)_2$·DEA, $Zn(OAc)_2$·TEA and $Zn(OAc)_2$·TEA/PEI complex solution

Zinc acetate dihydrate ($Zn(OAc)_2·2H_2O$) was first vacuum-dried heated at 100 °C for 12 h under vacuum to remove coordinated water, yielding anhydrous $Zn(OAc)_2$.

To prepare the $Zn(OAc)_2$·DEA complex, 459 mg (2.50 mmol) of $Zn(OAc)_2$ was dissolved in 5 mL of anhydrous EtOH. Separately, a DEA solution was prepared by dissolving 263 mg (2.50 mmol) of DEA in 2 mL of EtOH, which was added dropwise to the $Zn(OAc)_2$/EtOH solution under stirring at 50 °C. After complete dissolution and formation of a clear, colorless solution, EtOH was added to bring the final volume to 10 mL, yielding a 0.25 M $Zn(OAc)_2$·DEA complex solution.

To prepare the $Zn(OAc)_2$·TEA complex, 459 mg (2.50 mmol) of $Zn(OAc)_2$ was dispersed in 5 mL of NMP ($Zn(OAc)_2$ is insoluble on NMP). Separately, a TEA solution was prepared by dissolving 373 mg (2.50 mmol) of TEA in 2 mL of NMP, which was added dropwise to the $Zn(OAc)_2$ mixture under stirring at room temperature for 2 h. A clear, colorless $Zn(OAc)_2$·TEA complex solution was obtained, which was then diluted with additional NMP to a total volume of 10 mL to achieve a concentration of 0.25 M.

To prepare $Zn(OAc)_2$·TEA/PEI complex solutions with varying PEI contents (5, 10, 15, and 25 wt% based on the total mass of $Zn(OAc)_2$·TEA + PEI), designated as $Zn(OAc)_2$·TEA/PEI (5%), $Zn(OAc)_2$·TEA/PEI (10%), $Zn(OAc)_2$·TEA/PEI (15%) and $Zn(OAc)_2$·TEA/PEI (25%), the appropriate amount of PEI solution in NMP was added to the $Zn(OAc)_2$·TEA complex solution, followed by stirring for 12 h.

All the procedures were carried out inside an argon-filled glove box with O_2 and H_2O concentrations maintained below 0.5 ppm.

2.3 Synthesis of Li_2S_6

The Li_2S_6 solution was obtained by heating a mixture of Li_2S and elemental sulfur (S) with a molar ratio of 1 : 5 in a mixture solvent of 1,2-dimethoxyethane (DME) and 1,3-dioxolane (DOL) (v/v = 1 : 1) at 80 °C for 12 h under stirring. The Li_2S_6 solution was diluted to 0.5 M for further use.

2.4 Fabrication of lithium sulfide electrodes

A mixture of Li_2S, SP, and $Zn(OAc)_2$·TEA or $Zn(OAc)_2$·TEA/PEI at a mass ratio of 70 : 20 : 10 in anhydrous NMP was manually ground using a mortar for 30 min inside an argon-filled glove box with O_2 and H_2O concentrations maintained below 0.5 ppm. The resulting slurry was then applied to a carbon-coated aluminum foil using bar coating and dried at 50 °C under reduced pressure for 12 h inside the glovebox. After drying, the coated foil was punched into 12 mm diameter discs with a diameter of 12 mm and stored in sealed vials inside the glovebox. The Li_2S loading was 1.0–1.2 mg cm^{-2} for typical cells and ~4 mg cm^{-2} for high loading cells.

For comparison, control electrodes were fabricated using PVDF as the binder instead of $Zn(OAc)_2$·TEA or $Zn(OAc)_2$·TEA/PEI, following the same procedure.

2.5 Electrochemical measurements

2032 coin-type Li_2S-LSBs were assembled using the above prepared Li_2S cathodes, lithium metal anodes (0.45 mm thick foils with a diameter of 15.6 mm), Celgard 2400 separators, and an electrolyte consisting of 1 M lithium bis(trifluoromethanesulfonyl)imide (LiTFSI) in a 1 : 1 volume ratio of 1,3-dioxolane (DOL) and dimethoxyethane (DME), containing 2 wt% $LiNO_3$ as the electrolyte inside an argon-filled glovebox. The electrolyte volume was 24 μL. For high-loading Li_2S electrochemical performance tests, carbon paper was used as the substrate, and the electrolyte volume was 60 μL. The batteries were assembled using a manual hydraulic press at 1000 psi for 5 seconds. The electrochemical performance of the batteries was assessed through galvanostatic measurements performed on a Land 2001A battery test system. All capacities and cycling rates are calculated based on the mass of Li_2S, with 1 C defined as 1166 mA g^{-1} based on the theoretical capacity of Li_2S. Electrochemical impedance spectra (EIS) were recorded at the open-circuit potential (OCP) using a Biologic electrochemical potentiostat/galvanostat (VSP) over a frequency range of 1000 kHz to 0.1 Hz, with an alternating current (AC) amplitude of 10 mV. Cyclic voltammetry (CV) tests were carried out by initial charging between 1.7 and 4.0 V for the first cycle and the following cycles between 1.7 and 2.8 V at a scan rate of 0.025 mV s^{-1}.

2.6 Characterization

XRD measurements of Li_2S samples were carried out on a Bruker D8 Discover X-ray diffractometer using Cu K_α radiation (λ = 1.5418 Å). XRD samples were covered with Kapton tape to prevent them from absorbing moisture in the ambient air. UV–Vis absorption spectra were measured on a Cary 7000 universal measurement spectrophotometer (UMS). SEM images were taken using a Zeiss Sigma HD microscope.

3. Results and discussion

Preparation of $Zn(OAc)_2$·TEA complex

Previously, the $Zn(OAc)_2$·DEA complex, synthesized from Zn $(OAc)_2$·$2H_2O$ in a mixture of ethanol and water, was utilized as a multifunctional binder for S-LSBs, demonstrating superior LPS trapping capability for maintaining long-term cycling stability and an effective catalytic effect on the redox reactions of sulfur species to achieve high specific capacity and high rate capacibity.[42] However, this binder solution cannot be directly applied to Li_2S cathode preparation due to the high moisture sensitivity of Li_2S, which readily hydrolyzes to form LiOH. This necessitates the use of an anhydrous solvent to make the binder solution. While the $Zn(OAc)_2$·DEA complex can be dissolved in anhydrous ethanol at elevated temperatures (~50 °C), its limited solubility at room temperature presents practical difficulties. Moreover, Li_2S exhibits partial solubility in ethanol, and the resulting dissolved species react rapidly with Zn^{2+} in the complex, displacing acetate ligands and forming insoluble Zn–S species.[42] This leads to immediate gelation of the slurry, severely impairing electrode fabrication and processing.

To overcome these limitations, NMP was selected as the processing solvent due to its chemical inertness toward Li_2S.[23] However, $Zn(OAc)_2$·DEA is insoluble in NMP, limiting its practical use under these conditions. To address this issue, triethanolamine (TEA) was employed as an alternative ligand. The presence of an additional hydroxyl group in TEA renders the resulting $Zn(OAc)_2$·TEA complex soluble in NMP, as shown Fig. 1a. The XRD pattern of the vacuum-dried $Zn(OAc)_2$·TEA sample displayed distinct diffraction peaks, indicating its high crystallinity (Fig. 1b). The XRD pattern of the Li_2S/SP/Zn $(OAc)_2$·TEA sample obtained by drying the slurry (Fig. 1c) further confirms the homogeneous dispersion of Zn $(OAc)_2$·TEA within the composite.

The reaction between $Zn(OAc)_2$·DEA and LPSs has been documented in the previous study, which demonstrated that two polysulfide chains can replace the two acetate groups coordinated to Zn^{2+} in $Zn(OAc)_2$·DEA.[42] Given the close structural similarity between $Zn(OAc)_2$·TEA and $Zn(OAc)_2$·DEA, it is reasonable to expect comparable polysulfide-trapping capability from $Zn(OAc)_2$·TEA. To confirm this, an LPS trapping experiment was conducted by adding 2 molar equivalents of $Zn(OAc)_2$·TEA to 1 molar equivalent of Li_2S_6 dissolved in a DOL/DME (v/v = 1 : 1) electrolyte solvent (Fig. 1d). Upon the addition of $Zn(OAc)_2$·TEA, the characteristic dark color of Li_2S_6 quickly faded, accompanied by the formation of brown precipitates. This behavior closely resembles the previously observed reaction between $Zn(OAc)_2$·DEA and LPSs, suggesting that Zn $(OAc)_2$·TEA readily captures LPSs through a similar mechanism. The formation of insoluble $Zn(S_xLi)_2$·TEA species (x = 4 to 8) is expected to effectively suppress the polysulfide shuttle

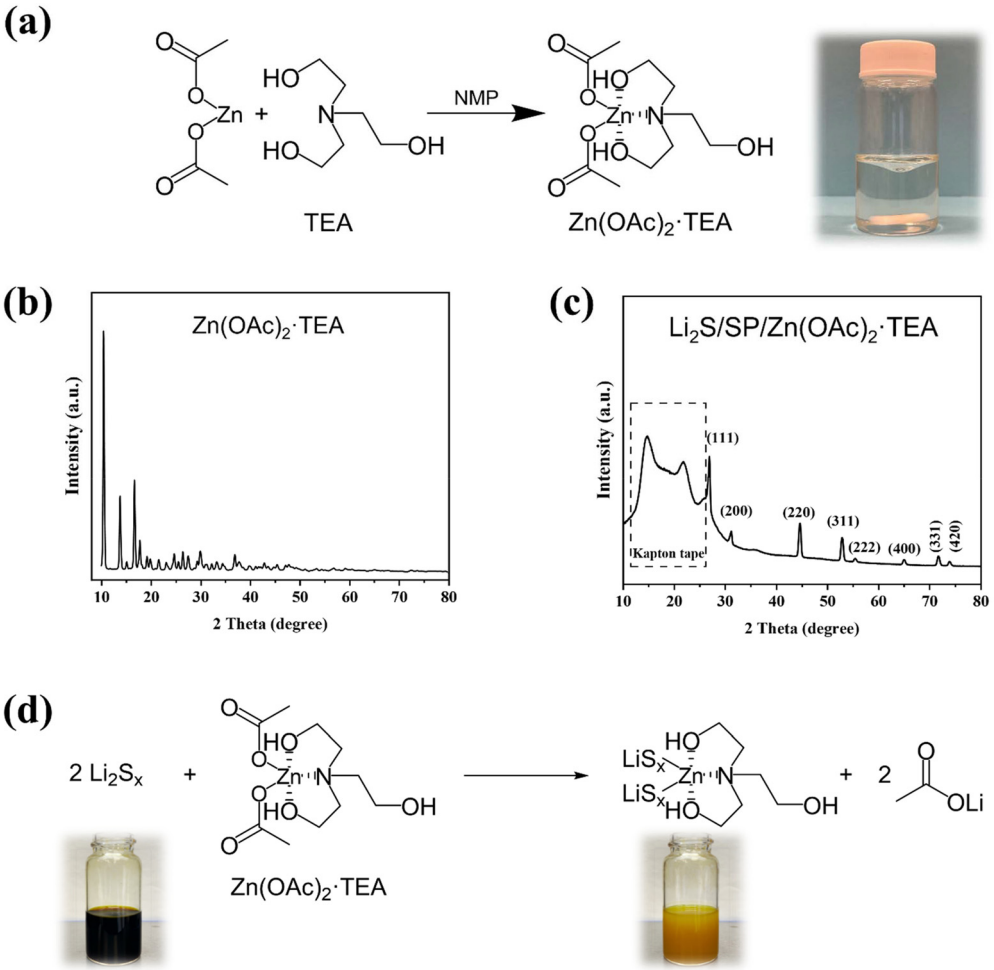

Fig. 1 (a) $Zn(OAc)_2$·TEA prepared by mixing anhydrous $Zn(OAc)_2$ and TEA mixed in NMP. (b) XRD pattern of vacuum-dried $Zn(OAc)_2$·TEA. (c) XRD pattern of Kapton tape-covered dried Li_2S/SP/$Zn(OAc)_2$·TEA mixture. (d) Reaction between $Zn(OAc)_2$·TEA and lithium polysulfides (Li_2S_x, where x = 4–8), with photographs showing a Li_2S_6 solution before and after the addition of 0.5 molar equivalents of $Zn(OAc)_2$·TEA inside a glove box. The dark red Li_2S_6 solution turned into a suspension with brown precipitates, indicating complete reaction.

effect. The molar trapping capacity of $Zn(OAc)_2$·TEA toward LPS was determined *via* UV–vis spectroscopy to be 1.975 mol LPS per mol $Zn(OAc)_2$·TEA as detailed in Fig. S1† and Table S2.† This result confirms the strong LPS-trapping capability of $Zn(OAc)_2$·TEA, with each binder unit effectively coordinating with two LPS species *via* interactions with Zn^{2+} centers —consistent with previous findings for the $Zn(OAc)_2$·DEA system.[42]

Electrochemical performance of $Zn(OAc)_2$·TEA-based Li_2S electrode

The galvanostatic cycling performance of Li_2S batteries employing $Zn(OAc)_2$·TEA and PVDF as binders is presented in Fig. 2a–e. During the initial activation process, the cells were cycled at a current density of 0.05 C (1 C = 1166 mA g^{-1}) (Fig. 2a). Both electrodes exhibited a pronounced overpotential spike at the onset of charging, followed by a gradual voltage decline, a behavior characteristic of Li_2S-LSBs.[23] The $Zn(OAc)_2$·TEA-based electrode displayed a lower activation spike of 3.55 V compared to that of the PVDF-based electrode (3.69 V), indicating that $Zn(OAc)_2$·TEA catalyzes Li_2S activation by lowering the energy barrier. Additionally, the $Zn(OAc)_2$·TEA-based electrode exhibited higher post-spike voltages compared to the PVDF-based counterpart. This is attributed to the strong LPS-trapping ability of $Zn(OAc)_2$·TEA, which immobilizes LPSs generated on the surface of Li_2S particles, preventing exposure of interior Li_2S to the electrolyte. As a result, further oxidation of Li_2S in the particle interior is hindered. In contrast, in the PVDF-based electrode, LPSs dissolve into the electrolyte, absorbing solvent to lower the activation barrier,[44] and diffuse away from the particle surface, thereby exposing fresh Li_2S for continued oxidation.

During the subsequent discharge, both electrodes delivered similar capacities in the first plateau (208.1 and 213.3 mA h g^{-1} for $Zn(OAc)_2$·TEA and PVDF, respectively), corresponding to the reduction of S_8 into long-chain polysulfides (Li_2S_x,

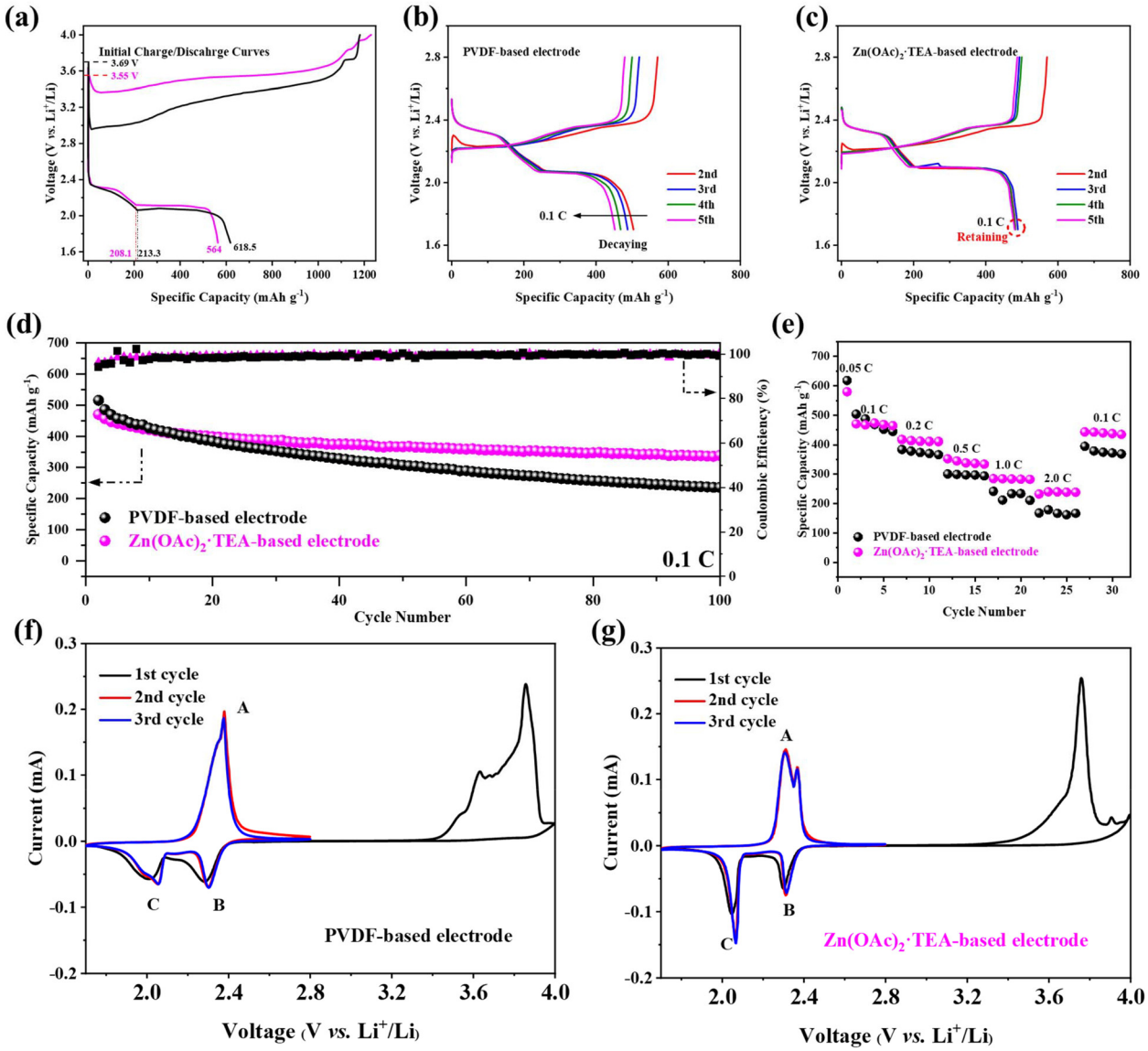

Fig. 2 Electrochemical performance of Li_2S electrodes using PVDF and $Zn(OAc)_2$·TEA as binders. (a) First-cycle charge/discharge curves at 0.05 C. (b and c) Initial five charge/discharge cycles of PVDF- and $Zn(OAc)_2$·TEA-based electrodes, respectively. (d) Cycling performance at 0.1 C. (e) Rate performance at various current densities. (f and g) Cyclic voltammetry (CV) curves of PVDF- and $Zn(OAc)_2$·TEA-based electrodes, respectively. Electrodes were scanned from 1.7 to 4.0 V for the first cycle, and from 1.7 to 2.8 V for subsequent cycles at a scan rate of 0.025 mV s^{-1}.

x = 4–8). However, in the second plateau, which involves the stepwise conversion of Li_2S_4 to Li_2S_2 and finally Li_2S, the Zn $(OAc)_2$·TEA-based cathode exhibited a significantly shorter plateau and a lower overall discharge capacity (564.0 mA h g^{-1} *vs.* 618.5 mA h g^{-1} for PVDF). This lower capacity is attributed to the immobilization of long-chain LPSs by $Zn(OAc)_2$·TEA, which restricts their diffusion and uniform distribution within the cathode, thereby impeding the solid-state conversion of Li_2S_2 to Li_2S. In contrast, in the PVDF-based cathode, the dissolved LPSs diffuse more freely, enabling better distribution and more complete conversion of Li_2S_2 to Li_2S. Unlike the thermally infiltrated S@SP nanocomposites used in Zn $(OAc)_2$·DEA-based S-LSBs, where sulfur is uniformly confined within mesoporous carbon, facilitating the Li_2S_2-to-Li_2S conversion,[42] the present study uses Li_2S/SP mixture made from physically ground commercial Li_2S powders and SP, resulting in micrometer-sized Li_2S particles located outside the SP network. In this case, the inability of PVDF to trap LPSs incidentally assists in Li_2S particle size reduction and a more complete discharge.

Despite its lower initial discharge capacity, the Zn $(OAc)_2$·TEA-based cathode demonstrated markedly improved cycling stability at 0.1 C in subsequent cycles (Fig. 2b and c). While the PVDF-based cathode experienced a sharp decline from 515.4 mA h g^{-1} in the second cycle to 235.8 mA h g^{-1} by the 100th cycle (45.8% retention), the $Zn(OAc)_2$·TEA-based

electrode showed a much slower decay, decreasing from 470.3 to 339.2 mA h g^{-1} (72.1% retention), highlighting the stabilizing effect of $Zn(OAc)_2$·TEA through effective LPS trapping.

Additionally, the $Zn(OAc)_2$·TEA-based electrode exhibited superior rate performance compared to its PVDF-based counterpart, as shown in Fig. 2g. Specifically, the capacity retention at 2 C relative to 0.1 C was 51% for the $Zn(OAc)_2$·TEA-based electrode, significantly higher than the value of 33% observed for the PVDF-based electrode. This enhanced rate capability suggests improved redox kinetics in the $Zn(OAc)_2$·TEA-based system, likely attributed to the catalytic effect of the complex, similar to the behavior previously reported for its analogue, $Zn(OAc)_2$·DEA.[42]

The cyclic voltammetry (CV) profiles of the $Zn(OAc)_2$·TEA-based and PVDF-based Li_2S electrodes are shown in Fig. 2f and g. Notably, their initial CV curves differ significantly from those observed in subsequent cycles. In both cases, the first CV scan was performed from the open-circuit voltage (OCV) up to 4.0 V to initiate the electrochemical activation of the Li_2S cathode. Due to the presence of a passivating Li_2O/LiOH surface layer and the high crystallinity and purity of Li_2S, the initial charge process exhibits a distinct electrochemical signature characterized by a high overpotential.[21,45–47] This activation behavior is characteristic of Li_2S-LSBs and is not observed in conventional S-LSBs. During the first charge, the PVDF-based electrode exhibited an onset potential of 3.45 V, followed by a broad peak at 3.63 V, and reached a maximum current at 3.86 V. In contrast, the $Zn(OAc)_2$·TEA-based electrode showed a lower onset potential of 3.34 V and a sharper oxidation peak at 3.76 V, indicating a reduced energy barrier for Li_2S activation. This improvement is likely due to the catalytic effect of Zn^{2+} centers in the $Zn(OAc)_2$·TEA complex, which can accommodate LPS intermediates and facilitate their oxidation.[42] However, unlike the PVDF-based electrode, this electrode lacked a distinct first oxidation peak and instead displayed a shoulder before the main peak, consistent with LPS immobilization raising the activation energy for oxidation of Li_2S near the surface.

In the subsequent discharge process, the $Zn(OAc)_2$·TEA-based electrode exhibited much sharper and slightly higher-voltage reduction peaks (2.31 and 2.07 V) compared to the PVDF-based electrode (2.30 and 2.05 V), indicating lower polarization and enhanced redox kinetics. During the second charge, the PVDF electrode exhibited a broad, merged oxidation peak at 2.38 V, whereas the $Zn(OAc)_2$·TEA-based electrode displayed two distinct peaks at lower potentials of 2.31 and 2.37 V. Notably, the first peak, corresponding to the oxidation of Li_2S to long-chain polysulfides (Li_2S_x), was more prominent than the second, associated with the further conversion of Li_2S_x to elemental sulfur (S_8), suggesting that the Zn $(OAc)_2$·TEA binder effectively promotes the initial oxidation step.

Overall, the CV results demonstrate that the $Zn(OAc)_2$·TEA binder exhibits notable catalytic effects, effectively lowering the activation barrier during the initial charge and accelerating the redox reactions of sulfur species in subsequent cycles. Compared to the PVDF binder, it results in reduced polarization and more well-defined redox features, underscoring its superior ability to facilitate conversion reactions of sulfur species.

To evaluate the redox catalytic activity of $Zn(OAc)_2$·TEA, Tafel slope analysis was performed using CV data. This technique is widely used to assess the kinetics of electrochemical reactions and estimate charge-transfer resistance by analyzing the relationship between overpotential and logarithmic current density.[48,49] The second CV cycle was selected for analysis, as the first cycle in Li_2S-based batteries typically involves an activation process that does not reflect stabilized electrochemical behavior. Tafel slopes were extracted from the linear regions of the overpotential *versus* log(current) plots near the major redox peaks, as shown in Fig. S2† and summarized in Table S3.† The results clearly demonstrate that the Zn $(OAc)_2$·TEA-based electrode exhibits significantly lower Tafel slopes compared to the control, indicating improved charge-transfer kinetics and enhanced redox catalytic activity.

These results collectively demonstrate that $Zn(OAc)_2$·TEA serves not only as a structural binder but also as a multifunctional additive that enhances battery performance through LPS trapping and redox catalysis. Its ability to immobilize LPSs helps suppress the shuttle effect and improves cycling stability, while its redox-active Zn^{2+} centers promote the initial activation of Li_2S and facilitate subsequent redox reactions. These combined effects provide significant advantages over the conventional PVDF binder. The improved electrochemical behavior of $Zn(OAc)_2$·TEA-based electrodes is believed to follow a mechanism analogous to that previously proposed for Zn $(OAc)_2$·DEA in S-LSBs.[42] A modified version tailored to the Zn $(OAc)_2$·TEA-based Li_2S cathode is illustrated in Fig. 3a, highlighting the trapping and release of sulfur species by the Zn^{2+} centers during the charge and discharge processes.

A key distinguishing feature of Li_2S-based cells is the initial charging process, which requires overcoming a high activation barrier due to the material's intrinsic crystallinity and the presence of a passivating LiOH/Li_2O surface layer (Fig. 3b). The Zn $(OAc)_2$·TEA molecules in contact with Li_2S particles can react with nascent LPSs and catalyze their oxidation, thereby reducing the overpotential compared to PVDF. However, because the trapped LPSs remain immobilized and do not dissolve into the electrolyte, subsequent oxidation of interior Li_2S becomes difficult, leading to elevated post-spike charging voltages.

During discharge, particularly in the later stage of the second plateau, significant volume expansion occurs as Li_2S_2 is reduced to Li_2S. The structural preservation effect of the Zn $(OAc)_2$·TEA binder inhibits this conversion near the particle core, where the intrinsically low electronic and ionic conductivity of Li_2S_2 limits charge transport. As a result, the full transformation to Li_2S is impeded, leading to a lower discharge capacity compared to the PVDF-based electrode.

Modification of $Zn(OAc)_2$·TEA with PEI

Although $Zn(OAc)_2$·TEA exhibits significantly improved solubility in NMP compared to $Zn(OAc)_2$·DEA, it was observed to crys-

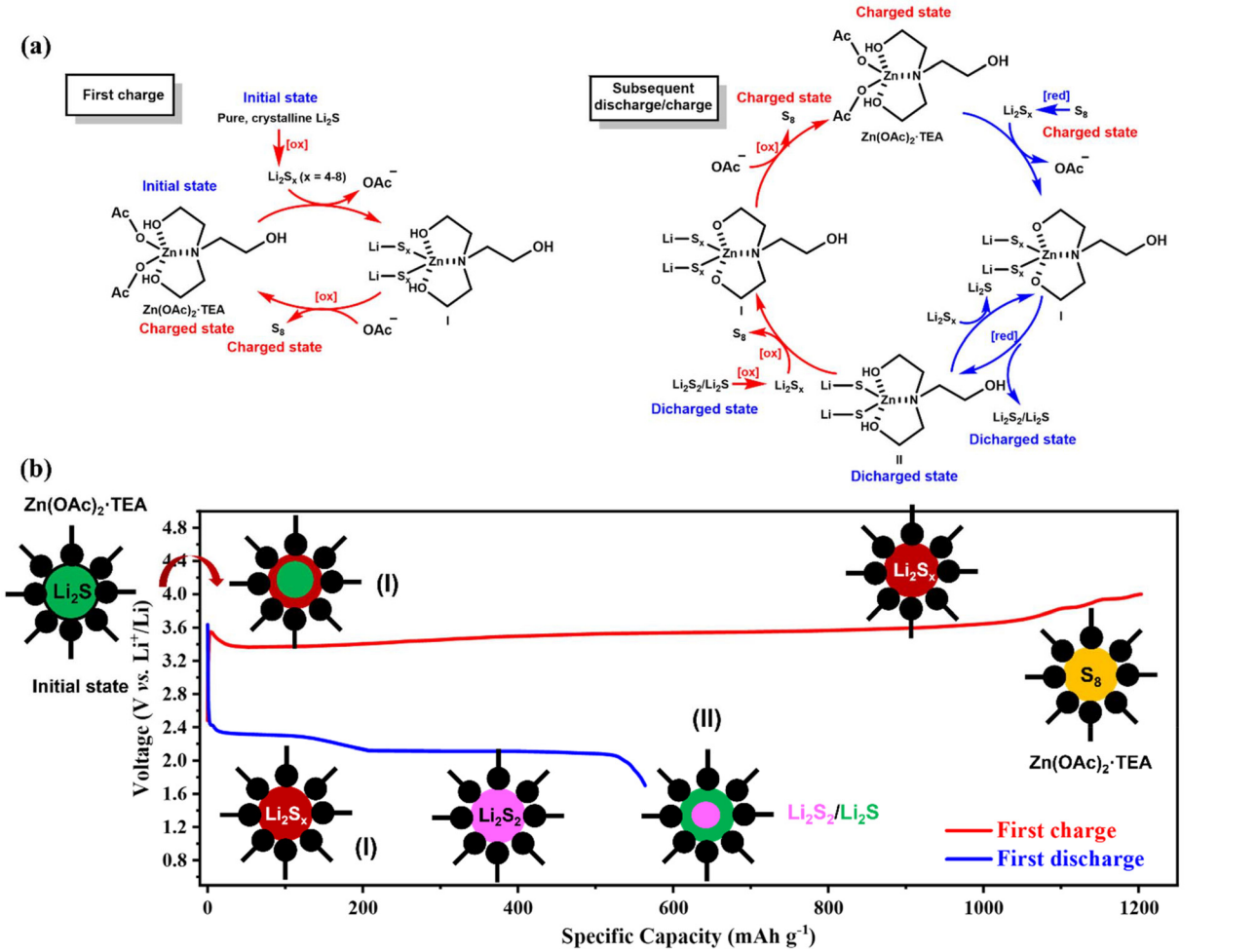

Fig. 3 (a) Proposed polysulfide trapping cycles of $Zn(OAc)_2$·TEA during the initial charge and subsequent discharge/charge processes in the Zn $(OAc)_2$·TEA-based Li_2S electrode ([red]: reduction; [ox]: oxidation). (b) Schematic representation of the structural evolution of Li_2S particles during the first charge/discharge cycle, corresponding to the stages illustrated in (a).

tallize upon standing for more than 12 h (Fig. S3†). This instability presents challenges for practical application and may compromise cathode quality due to potential aggregation of $Zn(OAc)_2$·TEA during electrode drying. In fact, at high current rates (*e.g.*, 2 C), the battery exhibited signs of overcharging (Fig. S4†), suggesting poor structural integrity of the cathode.

To address this issue, polyethylenimine (PEI) was introduced into the $Zn(OAc)_2$·TEA solution in NMP at various wt.% relative to $Zn(OAc)_2$·TEA/PEI (5%), $Zn(OAc)_2$·TEA/PEI (10%), Zn $(OAc)_2$·TEA/PEI (15%), and $Zn(OAc)_2$·TEA/PEI (25%). The rationale is that the nitrogen atoms in PEI can coordinate with Zn^{2+} centers in $Zn(OAc)_2$·TEA, analogous to the coordination observed with the nitrogen atoms in TEA and DEA. Since Zn^{2+} ions can accommodate up to six ligands,[50] it is plausible that one or two PEI-derived nitrogen atoms can bind to Zn^{2+}. In solution and during electrode drying, PEI may inhibit the crystallization or aggregation of $Zn(OAc)_2$·TEA. In the solid state, its polymeric structure can act as a cross-linker, facilitating the formation of a robust three-dimensional binder network that reinforces the structural integrity and stability of the cathode (Fig. 4).

It was found that white precipitates still formed in the Zn $(OAc)_2$·TEA/PEI (5%) solution after 12 h of storage, whereas solutions containing 10% or more PEI showed no visible precipitation after 12 h, as shown in Fig. S3,† and remained stable even upon storage for several months.

Electrochemical performance of $Zn(OAc)_2$·TEA/PEI-based Li_2S electrodes

Li_2S electrodes were fabricated using three binder solutions with varying PEI content: $Zn(OAc)_2$·TEA/PEI (10%), Zn $(OAc)_2$·TEA/PEI (15%), and $Zn(OAc)_2$·TEA/PEI (25%). Their galvanostatic charge/discharge profiles are shown in Fig. 5a–c. During the initial activation at 0.05 C, all three electrodes exhibited charge curves similar to that of the $Zn(OAc)_2$·TEA-based system (Fig. 2c). However, in the subsequent discharge, they delivered specific capacities of 596.7, 590.0, and

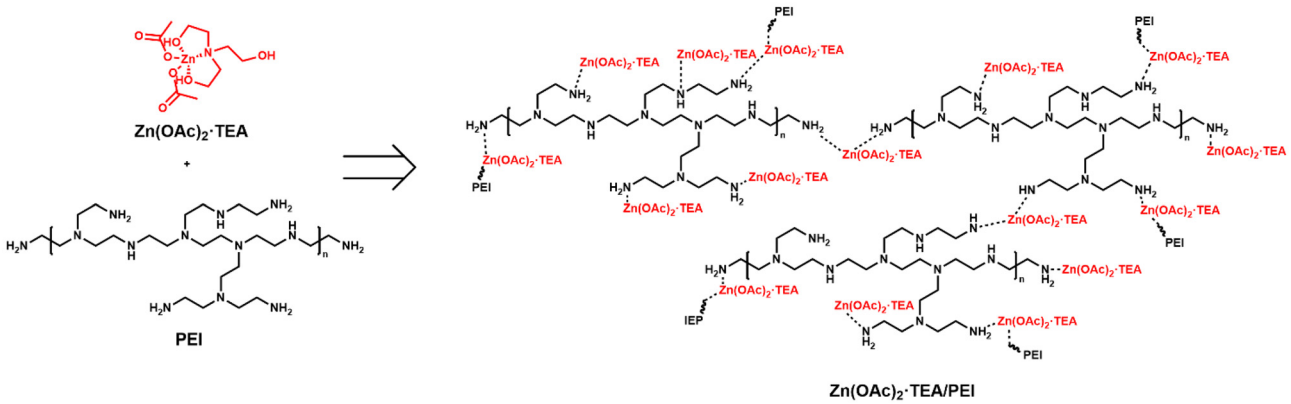

Fig. 4 Schematic illustration of the formation of the $Zn(OAc)_2$·TEA/PEI binder, where the addition of PEI enables the establishment of a three-dimensional (3D) network through coordination between Zn^{2+} ions in $Zn(OAc)_2$·TEA and nitrogen atoms in PEI.

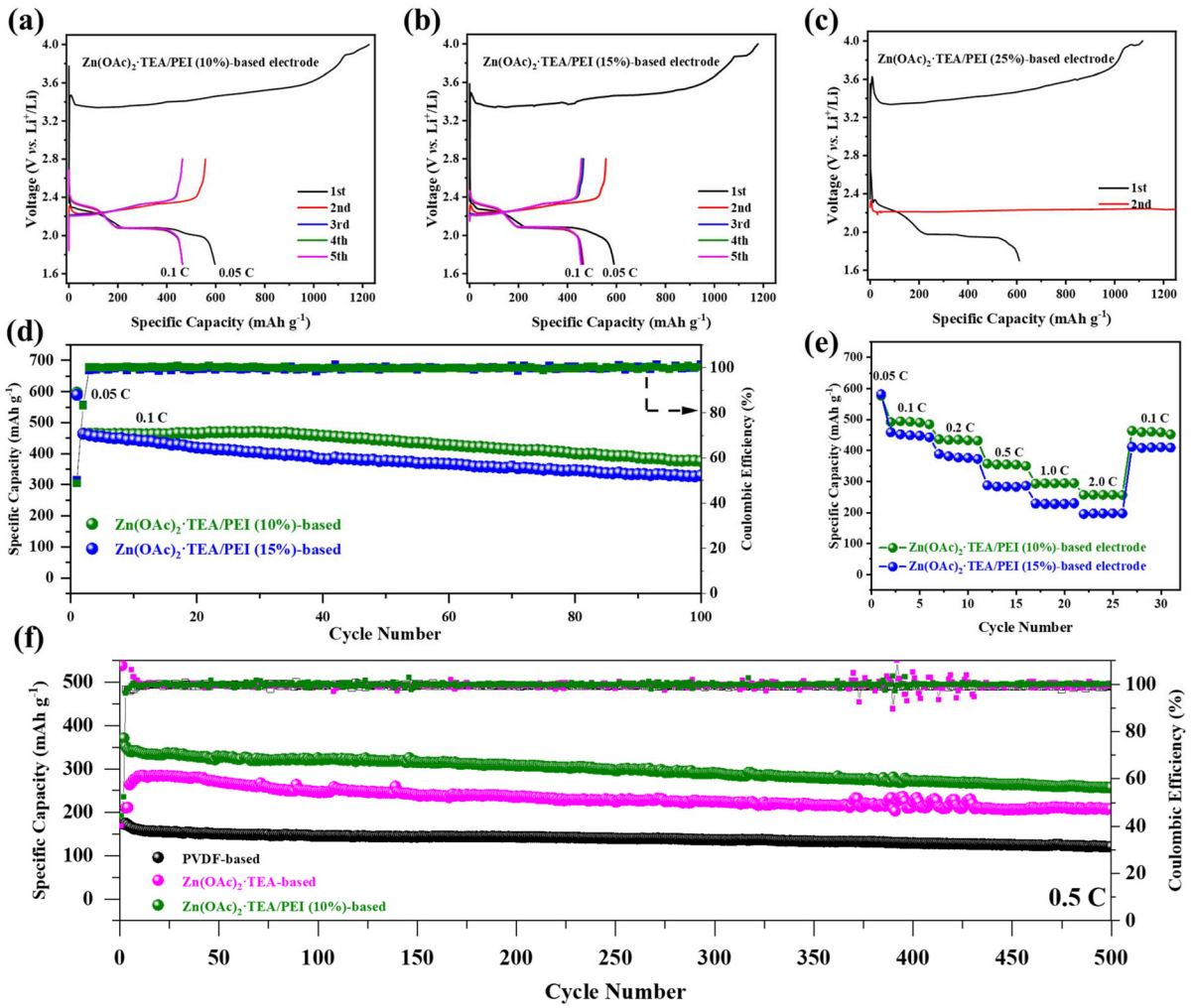

Fig. 5 Electrochemical performance of Li_2S electrodes using PVDF and various $Zn(OAc)_2$·TEA/PEI binders. (a) Initial five charge/discharge curves of $Zn(OAc)_2$·TEA/PEI (10%)-based electrode. (b) Initial five charge/discharge curves of $Zn(OAc)_2$·TEA/PEI (15%)-based electrode. (c) Initial charge/discharge curves $Zn(OAc)_2$·TEA/PEI (25%)-based electrode. (d) Cycling performance of the $Zn(OAc)_2$·TEA/PEI (10%)- and $Zn(OAc)_2$·TEA/PEI (15%)-based electrodes at 0.1 C. (e) Rate performance of the $Zn(OAc)_2$·TEA/PEI (10%)- and $Zn(OAc)_2$·TEA/PEI (15%)-based electrodes at various rates. (f) Long-term cycling performance of PVDF-, $Zn(OAc)_2$·TEA-, and $Zn(OAc)_2$·TEA/PEI (10%)-based electrodes at 0.5 C, which were all activated at 0.05 C in the first cycle.

610.0 mA h g^{-1}, respectively, each exceeding the 564.0 mA h g^{-1} capacity observed for the $Zn(OAc)_2$·TEA-based electrode. This improvement may be attributed to improved contact between Li_2S and Super P particles in the presence of flexible PEI chains.

At 0.1 C in the second cycle, the $Zn(OAc)_2$·TEA/PEI (10%)- and $Zn(OAc)_2$·TEA/PEI (15%)-based electrodes exhibited discharge profiles comparable to the $Zn(OAc)_2$·TEA-based electrode. However, the $Zn(OAc)_2$·TEA/PEI (25%)-based electrode showed signs of overcharging, suggesting mechanical or structural degradation within the cathode. A similar overcharging behavior was observed in the electrode using PEI alone as the binder (Fig. S5†), indicating that PEI lacks sufficient binding strength to preserve cathode integrity. In the 25% PEI formulation, excess or weakly crosslinked PEI may fail to adequately anchor Li_2S and Super P particles under a higher current density, leading to electrode instability and overcharging during charging.

Fig. 5d shows the cycling stability of the $Zn(OAc)_2$·TEA/PEI (10%)- and $Zn(OAc)_2$·TEA/PEI (15%)-based electrodes at 0.1 C. The $Zn(OAc)_2$·TEA/PEI (15%)-based electrode retained 70.3% of its initial capacity (in the second cycle) after 100 cycles, comparable to the 72.1% retention observed for the Zn $(OAc)_2$·TEA-based electrode. In contrast, the $Zn(OAc)_2$·TEA/PEI (10%)-based electrode exhibited improved stability, maintaining 81.0% of its capacity after 100 cycles.

The $Zn(OAc)_2$·TEA/PEI (10%)-based electrode also exhibited better high-rate capability than the $Zn(OAc)_2$·TEA/PEI (15%)-based electrode, as shown in Fig. 4e and Fig. S6.† The capacity retention at 2 C relative to 0.1 C was 52% for the 10% PEI formulation, compared to 43% for the 15% PEI counterpart. Notably, the rate capacity of the $Zn(OAc)_2$·TEA/PEI (10%)-based electrode is comparable to the $Zn(OAc)_2$·TEA-based electrode, indicating that the incorporation of 10% PEI (or a reduced content of Zn in the cathode) does not comprise the redox kinetics. As shown in Fig. S7,† the PVDF- and $Zn(OAc)_2$·TEA-based electrodes exhibited relatively unstable coulombic efficiencies during rate performance testing, especially when switching from low to high C-rates, indicating incomplete redox reactions or sluggish kinetics. In contrast, incorporating PEI into the $Zn(OAc)_2$·TEA binder markedly stabilized the coulombic efficiency across varying rates. This enhancement highlights PEI's role in improving charge transfer kinetics and maintaining reaction reversibility during rapid cycling.

The long-term cycling performance of the PVDF-, Zn $(OAc)_2$·TEA- and $Zn(OAc)_2$·TEA/PEI (10%)-based electrodes at a rate of 0.5 C is shown in Fig. 5f. After 500 cycles, the Zn $(OAc)_2$·TEA/PEI (10%)-based electrode retained a capacity of 256 mA h g^{-1} with a retention rate of 69.3%. In contrast, although the $Zn(OAc)_2$·TEA-based electrode initially delivered higher discharge capacities than the PVDF-based electrode, its capacity and Coulombic efficiency showed noticeable fluctuations between the 370th and 430th cycles, indicating structural degradation of the cathode. This instability is likely due to the limited binding strength of $Zn(OAc)_2$·TEA alone. The incorporation of 10% PEI significantly improved cathode stability, enabling sustained cycling and the highest overall discharge capacity among the three batteries. To evaluate the long-term cycling performance of high-loading Li_2S cathodes, two electrodes with areal loadings of 3.72 and 4.51 mg cm^{-2} were tested at 0.5 C as shown in Fig. S8.† For the 3.72 mg cm^{-2} electrode, the initial capacity was only 143 mA h g^{-1}, indicating incomplete activation of Li_2S likely due to increased internal resistance associated with higher loading. With continued cycling, gradual activation occurred, and the capacity increased to 187 mA h g^{-1} after 500 cycles. Similarly, the 4.51 mg cm^{-2} electrode exhibited a lower initial capacity of 95 mA h g^{-1}, but also showed continuous activation, reaching 147 mA h g^{-1} by the 500th cycle. These results highlight the challenges of fully activating Li_2S under high mass loading and high current density, while also demonstrating the structural and electrochemical robustness of the electrode during extended cycling.

Electrochemical impedance spectroscopy (EIS) results for freshly prepared PVDF-, $Zn(OAc)_2$·TEA-, $Zn(OAc)_2$·TEA/PEI (10%)-, and $Zn(OAc)_2$·TEA/PEI (15%)-, $Zn(OAc)_2$·TEA/PEI (25%)-based electrodes are presented in Fig. S9† and Table S4.† Among the $Zn(OAc)_2$·TEA and PEI-modified systems, the $Zn(OAc)_2$·TEA/PEI (10%)-based electrode exhibited the lowest charge transfer resistance (R_{ct} = 61.1 Ω), indicating improved interfacial charge transport. For comparison, the PVDF-based electrode showed the lowest R_{ct} value of 52.4 Ω, which is attributed to the removal of the insulating $LiOH/Li_2O$ layer on the Li_2S surface through its reaction with PVDF during slurry processing.[23]

EIS was also conducted on cycled electrodes using different binders as shown in Fig. S10† and Table S5.† All three electrodes exhibited Nyquist plots featuring two semicircles: the high-frequency semicircle associated with charge-transfer resistance (R_{ct}), and the medium-frequency semicircle corresponding to interfacial resistance (R_{int}) arising from Li_2S deposition and formation of other interfacial layers. Among the tested electrodes, the $Zn(OAc)_2$·TEA/PEI (10%)-based electrode exhibited the smallest R_{int}, followed by the $Zn(OAc)_2$·TEA-based electrode. In contrast, the PVDF-based electrode showed the largest impedance, reflecting poorer interfacial charge transfer and less effective suppression of polysulfide diffusion. These results suggest that the introduction of PEI into the Zn $(OAc)_2$·TEA matrix significantly improves the electrochemical environment at the electrode–electrolyte interface, likely due to enhanced ionic transport, better Li_2S redox reversibility, and stronger interactions with soluble polysulfides.

Mechanical integrity and structural evolution of PVDF-, $Zn(OAc)_2$·TEA-, and $Zn(OAc)_2$·TEA/PEI (10%)-based Li_2S electrodes

To evaluate the mechanical integrity and structural evolution of Li_2S cathodes with different binder systems, we performed both tape peeling tests and scanning electron microscopy (SEM) analysis.

As shown in Fig. S11,† the tape peeling tests provide a qualitative assessment of electrode adhesion and cohesion. The PVDF-based electrode exhibited strong adhesion to the current collector and good internal cohesion, with only

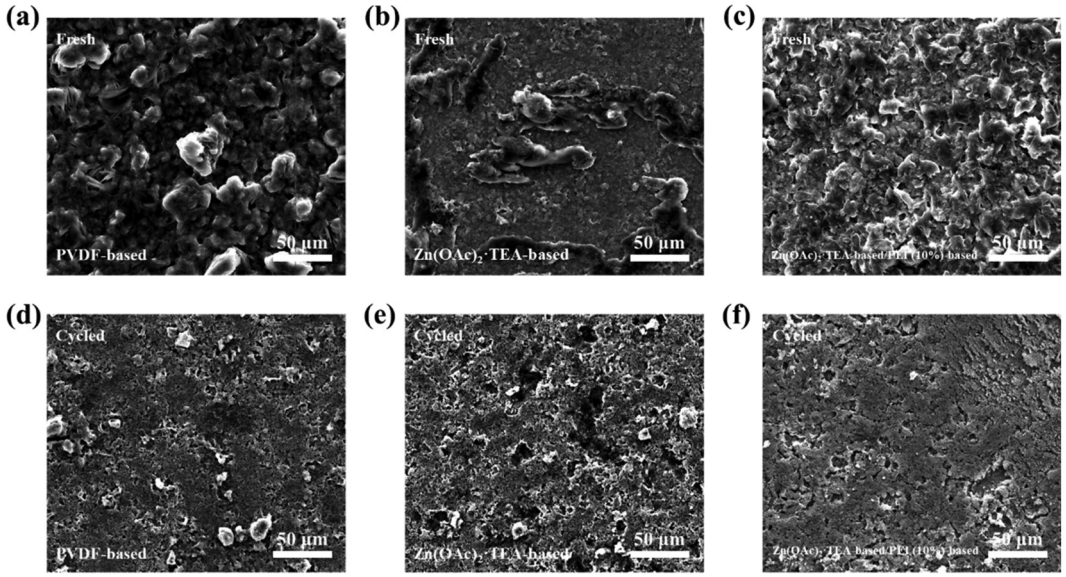

Fig. 6 SEM images of (a and d) PVDF-, (b and e) $Zn(OAc)_2$·TEA-, and (c and f) $Zn(OAc)_2$·TEA/PEI (10%)-based electrodes before and after 100 cycles.

minimal amounts of fine black powder transferred to the tape. In contrast, the $Zn(OAc)_2$·TEA-based electrode showed weaker mechanical integrity, likely due to the limited strength of hydrogen bonding between binder molecules. However, incorporating 10% PEI into the $Zn(OAc)_2$·TEA binder significantly improved mechanical stability, as evidenced by fewer and larger detached particles compared to both the $Zn(OAc)_2$·TEA- and PVDF-based electrodes. The high molecular weight PEI not only provides intrinsic mechanical strength but also introduces abundant amine groups capable of coordinating with Zn^{2+}, forming a denser and more cohesive network that reinforces internal bonding and improves adhesion to the current collector. This enhanced binding capability of the $Zn(OAc)_2$·TEA/PEI (10%) system directly correlates with the markedly improved electrochemical performance and cycling stability of the corresponding Li_2S cathodes.

SEM analysis was conducted to observe the morphological features of the electrodes before and after cycling in Fig. 6. In the fresh state, all electrodes show the presence of large Li_2S particles, consistent with the commercial Li_2S used. After 100 cycles at 0.5 C, clear differences were observed. The PVDF-based electrode retained numerous large, agglomerated particles, likely unreacted Li_2S, indicating poor sulfur utilization and limited structural stabilization. The $Zn(OAc)_2$·TEA-based electrode exhibited fewer large particles after cycling, suggesting improved Li_2S dispersion and utilization due to the strong interactions between the sulfur species and $Zn(OAc)_2$·TEA. Notably, the $Zn(OAc)_2$·TEA/PEI (10%)-based electrode showed the most homogeneous surface morphology, with finely distributed sulfur species and minimal residual large Li_2S particles. This reflects the synergistic effect of PEI, whose high molecular weight and abundant amine groups strengthen the binder network, enhancing structural integrity, suppressing particle aggregation, and improving Li_2S reversibility.

Conclusions

In this study, we developed a multifunctional, fluorine-free binder system based on a $Zn(OAc)_2$·TEA/PEI complex for high-performance lithium sulfide (Li_2S) cathodes in lithium–sulfur batteries. The $Zn(OAc)_2$·TEA complex exhibited strong lithium polysulfide (LPS) trapping capability and redox catalytic activity, which are critical for suppressing the polysulfide shuttle effect and promoting efficient Li_2S activation and conversion. However, the standalone use of $Zn(OAc)_2$·TEA posed issues related to crystallization and insufficient mechanical integrity during extended cycling. To address this, polyethylenimine (PEI) was introduced as a co-binder to form a stable hybrid binder network. The PEI not only enhanced solution processability and prevented binder crystallization, but also reinforced the structural integrity of the cathode through potential crosslinking with Zn^{2+} centers.

Electrochemical evaluations revealed that the optimized binder containing 10 wt% PEI, $Zn(OAc)_2$·TEA/PEI (10%), outperformed the widely used PVDF binder in terms of long-term cycling stability and rate capability. Overall, this work presents a rational binder design strategy that integrates chemical functionality with mechanical robustness to overcome the unique challenges of Li_2S cathodes. The successful use of a fluorine-free, metal–organic binder paves the way for more environmentally sustainable and scalable solutions for Li_2S-based lithium–sulfur batteries.

Author contributions

Zhe Huang: Conceptualization, data curation, formal analysis, investigation, methodology, validation, visualization, writing – original draft, writing – review & editing. Yonglin Wang: Data

curation, formal analysis, investigation. methodology. Yixuan Zhao: Data curation, formal analysis, investigation. methodology. Yuning Li: Conceptualization, formal analysis, funding acquisition, investigation, methodology, visualization, project administration, resources, supervision, writing – review & editing.

Conflicts of interest

The authors declare that they have no known competing financial interests or personal relationships that could have appeared to influence the work reported in this paper.

Data availability

The data supporting this article have been included as part of the ESI.†

Acknowledgements

The authors gratefully acknowledge financial support from the Natural Sciences and Engineering Research Council of Canada (NSERC) through a Discovery Grants (RGPIN-2022-03835) and an Alliance Grants (ALLRP 581429-23).

References

1 R. Dua, S. Almutairi and P. Bansal, *Energy Rep.*, 2024, **12**, 1836–1847.
2 H. Yuan, M. Ma, N. Zhou, H. Xie, Z. Ma, X. Xiang and X. Ma, *Appl. Energy*, 2024, **365**, 123153.
3 H. Niu, N. Zhang, Y. Lu, Z. Zhang, M. Li, J. Liu, N. Zhang, W. Song, Y. Zhao and Z. Miao, *J. Energy Storage*, 2024, **88**, 111666.
4 P. Albertus, S. Babinec, S. Litzelman and A. Newman, *Nat. Energy*, 2018, **3**, 16–21.
5 F. Wu, J. Maier and Y. Yu, *Chem. Soc. Rev.*, 2020, **49**, 1569–1614.
6 Z. Zhu, T. Jiang, M. Ali, Y. Meng, Y. Jin, Y. Cui and W. Chen, *Chem. Rev.*, 2022, **122**, 16610–16751.
7 J. Lu, Z. Chen, F. Pan, Y. Cui and K. Amine, *Electrochem. Energy Rev.*, 2018, **1**, 35–53.
8 Y. Tian, G. Zeng, A. Rutt, T. Shi, H. Kim, J. Wang, J. Koettgen, Y. Sun, B. Ouyang, T. Chen, Z. Lun, Z. Rong, K. Persson and G. Ceder, *Chem. Rev.*, 2021, **121**, 1623–1669.
9 C. P. Grey and D. S. Hall, *Nat. Commun.*, 2020, **11**, 6279.
10 Y. Fei and G. Li, *Adv. Funct. Mater.*, 2024, **34**, 2312550.
11 A. Manthiram, Y. Fu, S.-H. Chung, C. Zu and Y.-S. Su, *Chem. Rev.*, 2014, **114**, 11751–11787.
12 R. Deng, M. Wang, H. Yu, S. Luo, J. Li, F. Chu, B. Liu and F. Wu, *Energy Environ. Mater.*, 2022, **5**, 777–799.
13 W. Yao, J. Xu, L. Ma, X. Lu, D. Luo, J. Qian, L. Zhan, I. Manke, C. Yang, P. Adelhelm and R. Chen, *Adv. Mater.*, 2023, **35**, 2212116.
14 Z. Hao, Q. Zhao, J. Tang, Q. Zhang, J. Liu, Y. Jin and H. Wang, *Mater. Horiz.*, 2021, **8**, 12–32.
15 J. Wang, S. Yi, J. Liu, S. Sun, Y. Liu, D. Yang, K. Xi, G. Gao, A. Abdelkader, W. Yan, S. Ding and R. V. Kumar, *ACS Nano*, 2020, **14**, 9819–9831.
16 M. Abdollahifar, P. Molaiyan, U. Lassi, N. L. Wu and A. Kwade, *Renewable Sustainable Energy Rev.*, 2022, **169**, 112948.
17 Z. Hao, J. Chen, L. Yuan, Q. Bing, J. Liu, W. Chen, Z. Li, F. R. Wang and Y. Huang, *Small*, 2019, **15**, 1902377.
18 J. Hassoun and B. Scrosati, *Angew. Chem.*, 2010, **122**, 2421–2424.
19 J. Jiang, Q. Fan, S. Chou, Z. Guo, K. Konstantinov, H. Liu and J. Wang, *Small*, 2021, **17**, 1903934.
20 M. Li, Z. Chen, T. Wu and J. Lu, *Adv. Mater.*, 2018, **30**, 1801190.
21 Y. Son, J.-S. Lee, Y. Son, J.-H. Jang and J. Cho, *Adv. Energy Mater.*, 2015, **5**, 1500110.
22 S. Luo, F. Wu and G. Yushin, *Mater. Today*, 2021, **49**, 253–270.
23 Z. Huang, X. Gao, Y. Wang and Y. Li, *J. Power Sources*, 2023, **582**, 233530.
24 Z. Huang, Y. Wang and Y. Li, *ACS Appl. Energy Mater.*, 2025, **8**, 5759–5769.
25 H. Yuan, J.-Q. Huang, H.-J. Peng, M.-M. Titirici, R. Xiang, R. Chen, Q. Liu and Q. Zhang, *Adv. Energy Mater.*, 2018, **8**, 1802107.
26 S. K. Kannan, J. Joseph and M. G. Joseph, *Energy Fuels*, 2023, **37**, 6302–6322.
27 S. Tiwari, D. Pal, V. Yadav, D. Singh and A. K. Poonia, *Inorg. Chem. Commun.*, 2025, **177**, 114332.
28 R. Guo, Y. Yang, X. L. Huang, C. Zhao, B. Hu, F. Huo, H. K. Liu, B. Sun, Z. Sun and S. X. Dou, *Adv. Funct. Mater.*, 2024, **34**, 2307108.
29 N. D. Tyrrell, *Org. Process Res. Dev.*, 2023, **27**, 1422–1426.
30 F. Spyrakis and T. A. Dragani, *Toxics*, 2023, **11**, 721.
31 M. Zhao, H.-J. Peng, B.-Q. Li and J.-Q. Huang, *Acc. Chem. Res.*, 2024, **57**, 545–557.
32 L. Zhou, D. L. Danilov, F. Qiao, J. Wang, H. Li, R.-A. Eichel and P. H. L. Notten, *Adv. Energy Mater.*, 2022, **12**, 2202094.
33 Z. Cheng, H. Pan, H. Zhong, Z. Xiao, X. Li and R. Wang, *Adv. Funct. Mater.*, 2018, **28**, 1707597.
34 L. Yan, X. Gao, J. P. Thomas, J. Ngai, H. Altounian, K. T. Leung, Y. Meng and Y. Li, *Sustainable Energy Fuels*, 2018, **2**, 1574–1581.
35 X. Tao, J. Wang, C. Liu, H. Wang, H. Yao, G. Zheng, Z. W. Seh, Q. Cai, W. Li, G. Zhou, C. Zu and Y. Cui, *Nat. Commun.*, 2016, **7**, 11203.
36 G. Cheung and C. Huang, *Batteries*, 2025, **11**, 139.
37 X. Liang, C. Hart, Q. Pang, A. Garsuch, T. Weiss and L. F. Nazar, *Nat. Commun.*, 2015, **6**, 5682.
38 Q. Gong, L. Hou, T. Li, Y. Jiao and P. Wu, *ACS Nano*, 2022, **16**, 8449–8460.

39 Y. Liu, X. Meng, Z. Wang and J. Qiu, *Sci. Adv.*, 2022, **8**, eabl8390.
40 P. Han, S.-H. Chung, C.-H. Chang and A. Manthiram, *ACS Appl. Mater. Interfaces*, 2019, **11**, 17393–17399.
41 Q. Qi, X. Lv, W. Lv and Q.-H. Yang, *J. Energy Chem.*, 2019, **39**, 88–100.
42 Z. Ma, Z. Zuo and Y. Li, *ACS Appl. Mater. Interfaces*, 2021, **13**, 23936–23944.
43 Z. Ma, Z. Zuo, L. Li and Y. Li, *Adv. Funct. Mater.*, 2022, **32**, 2108692.
44 Y. Yang, G. Zheng, S. Misra, J. Nelson, M. F. Toney and Y. Cui, *J. Am. Chem. Soc.*, 2012, **134**, 15387–15394.
45 Y. Jung and B. Kang, *Phys. Chem. Chem. Phys.*, 2016, **18**, 21500–21507.
46 L. Zhang, D. Sun, J. Feng, E. J. Cairns and J. Guo, *Nano Lett.*, 2017, **17**, 5084–5091.
47 X. Li, M. Gao, W. Du, B. Ni, Y. Wu, Y. Liu, C. Shang, Z. Guo and H. Pan, *J. Mater. Chem. A*, 2017, **5**, 6471–6482.
48 K. Wang, Y. Wang, J. Wang, H. Wang, C. Ding, Z. Zheng, Y. Liu, Z. Luo and Y. Ding, *Adv. Funct. Mater.*, 2025, **35**, 2422689.
49 H. Xiao, K. Li, T. Zhang, X. Liang, F. Zhang, H. Zhuang, L. Zheng and Q. Gao, *Chem. Eng. J.*, 2023, **471**, 144553.
50 Y. Kondratenko, V. Fundamensky, I. Ignatyev, A. Zolotarev, T. Kochina and V. Ugolkov, *Polyhedron*, 2017, **130**, 176–183.